ORIGINAL RESEARCH

Nitrogen monoxide storage and sensing applications of transition metal–doped boron nitride nanotubes: a DFT investigation

Suphawarat Phalinyot[1] · Chanukorn Tabtimsai[2] · Banchob Wanno[1]

Abstract

The structural properties, electronic properties, and adsorption abilities for nitrogen monoxide (NO) molecule adsorption on pristine and transition metal (TM = V, Cr, Mn, Nb, Mo, Tc, Ta, W, and Re) doping on B or N site of armchair (5,5) single-walled boron nitride nanotube (BNNT) were investigated using the density functional theory method. The binding energies of TM-doped BNNTs reveal that the Mo atom doping exhibits the strongest binding ability with BNNT. In addition, the NO molecule weakly interacts with the pristine BNNT, whereas it has a strong adsorption ability on TM-doped BNNTs. The increase in the adsorption ability of NO molecule onto the TM-doped BNNTs is due to the geometrical deformation on TM doping site and the charge transfer between TM-doped BNNTs and NO molecule. Moreover, a significant decrease in energy gap of the BNNT after TM doping is expected to be an available strategy for improving its electrical conductivity. These observations suggest that NO adsorption and sensing ability of BNNT could be greatly improved by introducing appropriate TM dopant. Therefore, TM-doped BNNTs may be a useful guidance to be storage and sensing materials for the detection of NO molecule.

Keywords Adsorption · Boron nitride nanotube · DFT · Nitrogen monoxide · Transition metal

Introduction

The monitoring and storing of toxic gas in environment are considered as an important issue and many researches have been focused on the development of gas sensing materials for continuous monitoring [1–3]. Nitrogen monoxide (NO) is one of the major contributes to the air pollutants, which is generally produced from combustion of chemical processing and

✉ Banchob Wanno
  banchobw@gmail.com

1 Center of Excellence for Innovation in Chemistry and Supramolecular Chemistry Research Unit, Department of Chemistry, Faculty of Science, Mahasarakham University, Maha Sarakham 44150, Thailand

2 Computational Chemistry Center for Nanotechnology and Department of Chemistry, Faculty of Science and Technology, Rajabhat Maha Sarakham University, Maha Sarakham 44150, Thailand

fossil fuels in industrial. It destructs the ecological environment and harms human health. Additionally, it is also a cause of acid rain formation, photochemical smog, and ozone layer depletion [4, 5]. Several investigations have been observed to reduce or remove of NO molecules [6–8]. Therefore, the development of efficient nanomaterials to detect and remove NO molecules is greatly important.

Recently, the BN-based nanomaterials including boron nitride nanotubes (BNNTs) have attracted considerable attention as a promising material for gas detections [9–11]. Boron nitride nanotubes were first predicted through the binding calculation in 1994 [13, 14] and first synthesized via the arc-discharge method in the following year [15]. Subsequently, several investigations both theoretically and experimentally concerning the properties of these materials have been implemented [16–18]. Due to the unique and outstanding properties such as excellent mechanical resistance [19], low dielectric constant [20], and high thermal conductivity [21] as well as great chemical stability especially under hazardous, oxidative, and high-temperature environment [22], BNNTs have been promising potentials for the nanotechnology applications [23, 24]. Moreover, BNNTs exhibit ionic properties, due to

the electrophilic boron and nucleophilic nitrogen atoms of B–N bonds, which make their aqueous dispersibility and also non-cytotoxicity. The BNNTs may have potential applications in the biological system that the toxicity of carbon nanotubes (CNTs) is a problem [25]. Despite all these favorable properties presented, BNNTs also show a good surface area/volume ratio that can intrinsically act as sensor for toxic gas detections [26]. However, these features of BNNTs are the insulator or wide band gap semiconductor of about 5–6 eV, which is almost independent of the tube diameter, chirality, and number of walls [14, 27]. Owing to the uniform semiconducting behavior, BNNTs are inert to gas adsorptions [28, 29]. Therefore, it is important to overcome this increase the sensitivity for detecting and adsorbing molecular species with the nanostructures.

The sensitivity of BNNTs can be considerably enhanced though doping modification [30]. In the process of modifications, transition metal (TM) atom doping into BNNTs has been investigated to be an effective method for improving the electronic properties and increasing their chemical reactivities toward gas adsorptions [31]. The molecular adsorption of TM doping on BNNTs for experimental investigations shows that the hydrogen storage capacity in BNNTs is 2.6 wt%, while Pt atom doping on BNNTs can reach to be 4.2 wt% at room temperature [32]. Concerning the effects of NO adsorption on the dopant impurity into BNNTs for theoretical studies reveals that V, Cr, and Mn doping on BNNTs can enhance the conductivity and reduce the band gap of BNNTs [33]. The ability of TM atom (TM = V, Cr, Mn, Fe, Co, Ni) doping on BNNT to chemically adsorb the NO molecule was greatly increased in relation to that of the pristine BNNT [34]. Similarly, Wang and co-workers reported that the doping of Ge atom can significantly increase the strength of interaction between NO molecule and BNNT and also modify the geometrical structure of BNNT [35]. These previous works have indicated that doping BNNTs by introducing with impurity or TM atoms can significantly improve the electronic properties and adsorption abilities of BNNTs for the detection of many molecules, such as, H_2 [36], CO [10], CO_2 [26], SO_2 [9], N_2O [12], NO_2 [11], NH_3 [28], CH_4 [37], CNCl [29], and $COCl_2$ [30].

However, the interactions of BNNT doped with 3d (V, Cr, Mn), 4d (Nb, Mo, Tc), and 5d (Ta, W, Re) transition metal atoms and their adsorption with NO molecule have not been previously reported. To the best of our knowledge, the geometrical structures and binding energies of TM atoms doping on BNNT were calculated. Moreover, the geometrical structures, adsorption energies, and electronic properties of NO adsorption on the pristine and TM-doped BNNTs have been investigated in the present work. The results of this study may be also very important for the development of novel BNNT-based nanodevices acting as gas sensors or adsorptions.

Computational details

An armchair single-walled (5, 5) BNNT consisting of 45 boron, 45 nitrogen, and 20 hydrogen atoms ($B_{45}N_{45}H_{20}$) was modeled and computed. Hydrogen atoms were used to saturate the boron and nitrogen atoms at the two ends of the nanotube to avoid the boundary effects. For the transition metal-doped boron nitride nanotubes (TM-doped BNNTs), a single boron (B site) or nitrogen atom (N site) of BNNT in the middle of the nanotube was replaced with 3d (V, Cr, Mn), 4d (Nb, Mo, Tc), and 5d (Ta, W, Re) TM atoms to form V-, Cr-, Mn-, Nb-, Mo-, Tc-, Ta-, W-, and Re-doped BNNT systems. There are two different types of doping sites on BNNT, i.e. TM_B-doped BNNTs and TM_N-doped BNNTs, which were composed of TM–$B_{44}N_{45}H_{20}$ or TM–$B_{45}N_{44}H_{20}$, respectively. The adsorbed nitrogen monoxide (NO) molecule has been set over two possible adsorption sites of TM_B-doped BNNTs and TM_N-doped BNNTs. The geometry optimizations of the pristine and TM-doped BNNTs, and their adsorptions with NO molecule were performed using the density functional theory (DFT) method with the Lee–Yang−Parr correlational (B3LYP) [38–40] and the intensive Los Alamos LanL2DZ split−valence basis set [41, 42]. The B3LYP/LanL2DZ method was used because this method and basis set were successfully utilized for many studied systems [43–46]. Electronic properties, including the highest occupied molecular orbital (HOMO), the lowest unoccupied molecular orbital (LUMO), the energy gaps (E_g), the partial charge transfers (PCTs), and the total density of states (DOSs) upon pristine and TM-doped BNNTs, and their NO adsorptions were also studied at the same theoretical level. The energy gap was obtained from the difference between HOMO and LUMO energies. Meanwhile, the DOSs were estimated from the eigenvalues generated with single-point calculations, by using the following equation: $DOS = \sum_{i=1}^{N} occ(i) \exp\left\{-(E - C_i)^2\right\}$, where N and $occ(i)$ are the number of orbitals with a total energy (E) and occupation, respectively, and C_i is the vector of eigenvalues of the molecular orbitals. The PCTs during gas adsorptions can provide a definitive description for a change in electron charges of gas molecule during the adsorption process using the natural bond orbital (NBO) analysis [47] implemented in GAUSSIAN 09 program suite [48]. The molecular graphics of all related species were generated with the MOLEKEL 4.3 program [49]. The GaussSum 2.1.4 program [50] was used to get the DOS plots of all systems. The binding energies (E_b) of TM-doped BNNTs were calculated by the following equation:

$$E_b = E_{TM–BNNT} - (E_{BNNT} + E_{TM}) \tag{1}$$

where $E_{TM-BNNT}$, E_{BNNT}, and E_{TM} are the total energies of TM-doped BNNT, monovacant BNNT, and free metal, respectively.

The adsorption energies (E_{ads}) of a NO molecule adsorbed on the pristine and TM-doped BNNTs were defined as follows:

$$E_{ads} = E_{NO/BNNT} - (E_{BNNT} + E_{NO}) \qquad (2)$$

$$E_{ads} = E_{NO/TM-BNNT} - (E_{TM-BNNT} + E_{NO}) \qquad (3)$$

where $E_{NO/BNNT}$ and $E_{NO/TM-BNNT}$ are the total energies of NO adsorbed on pristine and TM-doped BNNTs, respectively. E_{BNNT} and $E_{TM-BNNT}$ are the total energies of the pristine and TM-doped BNNTs, respectively, and E_{NO} is the total energies of the isolated NO molecule. The lowest-energy structural configurations were chosen to compute the E_{ads} value and other properties for their adsorptions with NO molecule.

Conceptual DFT offers the global reactivity indices, which can be used to understand the chemical processes of the studied systems. Several of these indices are considered for chemical phenomena such as chemical potential (μ) and chemical hardness (η), which are defined as the first- and second-order partial derivatives of the system energy (E) regarding to the number of electron (N) at a constant external potential ($\upsilon(r)$), respectively [51]. The chemical potential and hardness were evaluated using the Koopmans' theorem as the follows [52]:

$$\mu = \left(\frac{\partial E}{\partial N} \right)_{\upsilon(\vec{r}),T} \cong \frac{(\varepsilon_H + \varepsilon_L)}{2} \qquad (4)$$

$$\eta = \frac{1}{2} \left(\frac{\partial^2 E}{\partial N^2} \right)_{\upsilon(\vec{r}),T} \cong \frac{(\varepsilon_L - \varepsilon_H)}{2} \qquad (5)$$

where ε_H and ε_L denote the energies of HOMO and LUMO, respectively.

An electrophilicity index (ω) which is proposed by Parr et al. [53] in terms of the chemical potential and chemical hardness can be written as the following equation:

$$\omega = \frac{\mu^2}{2\eta} \qquad (6)$$

Results and discussion

Geometrical structures of pristine and TM-doped BNNTs and their NO adsorptions

The B3LYP/LanL2DZ-optimized structure of the pristine BNNT is depicted in Fig. 1a. After full relaxation, the N1–

B3, N2–B3, and N3–B3 bond lengths are estimated to be 1.455, 1.455, and 1.454 Å, respectively. These results are comparable with the values reported by Paura and co-authors, in which the calculated B–N bond lengths of approximately 1.460 Å were obtained for the (5,5) armchair BNNT [26]. While the N1–B3–N2, N2–B3–N3, and N1–B3–N3 bond angles are estimated to be 119.8, 119.3, and 119.3°, respectively. Upon doping of TM atom on nanotube surface, doping site on either its B or N atom of BNNT is replaced with a TM atom (V, Cr, Mn, Nb, Mo, Tc, Ta, W, or Re atom). The TM atom forms three bonds with the nearest B or N atom, in which it alternates to sp^3 character. The calculated bond lengths between the TM atoms and its neighboring three N or B atoms are in the range of 1.812–1.985 Å and 1.941–2.232 Å for the TM_B-doped BNNTs and TM_N-doped BNNTs, respectively. It could be noted here that the TM–N bond lengths are obviously shorter than that of the TM–B bond lengths, indicating that the attraction of N atom with more electronegative is larger than that of the B atom. Furthermore, for almost TM_B-doped BNNT systems, the bond lengths along the tube axis TM–N1 or TM–N2 bond are all longer than the bond lengths with the other adjacent off-axis TM–N3 bond due to the tube curvature effect. Also, the bond angles of N–TM–N (92.5–104.4°) for TM_B-doped BNNTs are more enlarge than that B–TM–B (71.0–86.0°) for TM_N-doped BNNTs. Thus, the TM atoms on the surface of nanotube at N site are greater structural deformation than at B site, as it is clear from Figs. 2 and 3. It also notices that the bond angles of TM-doped BNNTs are narrower than those of the N–B–N or B–N–B bond angles of pristine BNNT. Comparing the geometrical structure, the TM atom introduces dramatically deformation of the tube surface near the doping site of BNNT to reduce stress. The impurity TM atoms protrude out of the tube wall due to the atomic radius for TM atoms larger than those of B and N atoms. The exterior change of the wall facilitates this region to enhance the reactivity, and it is expected that the present results play an especial important role in gas adsorption [12, 28–31].

Subsequently, the selected geometrical parameters of all possible adsorption configurations for NO adsorption on the pristine and TM-doped BNNTs are listed in Tables S1 and S2 in the Supplementary material section. The NO molecule is able to be adsorbed onto the tube surface via two different orientations, namely, though its N and O atoms. For simplicity, the N atom of NO molecule pointing toward the pristine BNNT and TM-doped BNNT is denoted by NO/BNNT and NO/TM-doped BNNT, respectively. Correspondingly, the O atom of NO molecule pointing toward the pristine BNNT and TM-doped BNNT is denoted by NO/BNNT and NO/TM-doped BNNT, respectively. In the most stable configurations of NO/BNNT, the adsorption distances (ADs) between NO molecule and the pristine BNNT are 3.000 and 2.932 Å when pointing its N and O atoms toward the adsorption site,
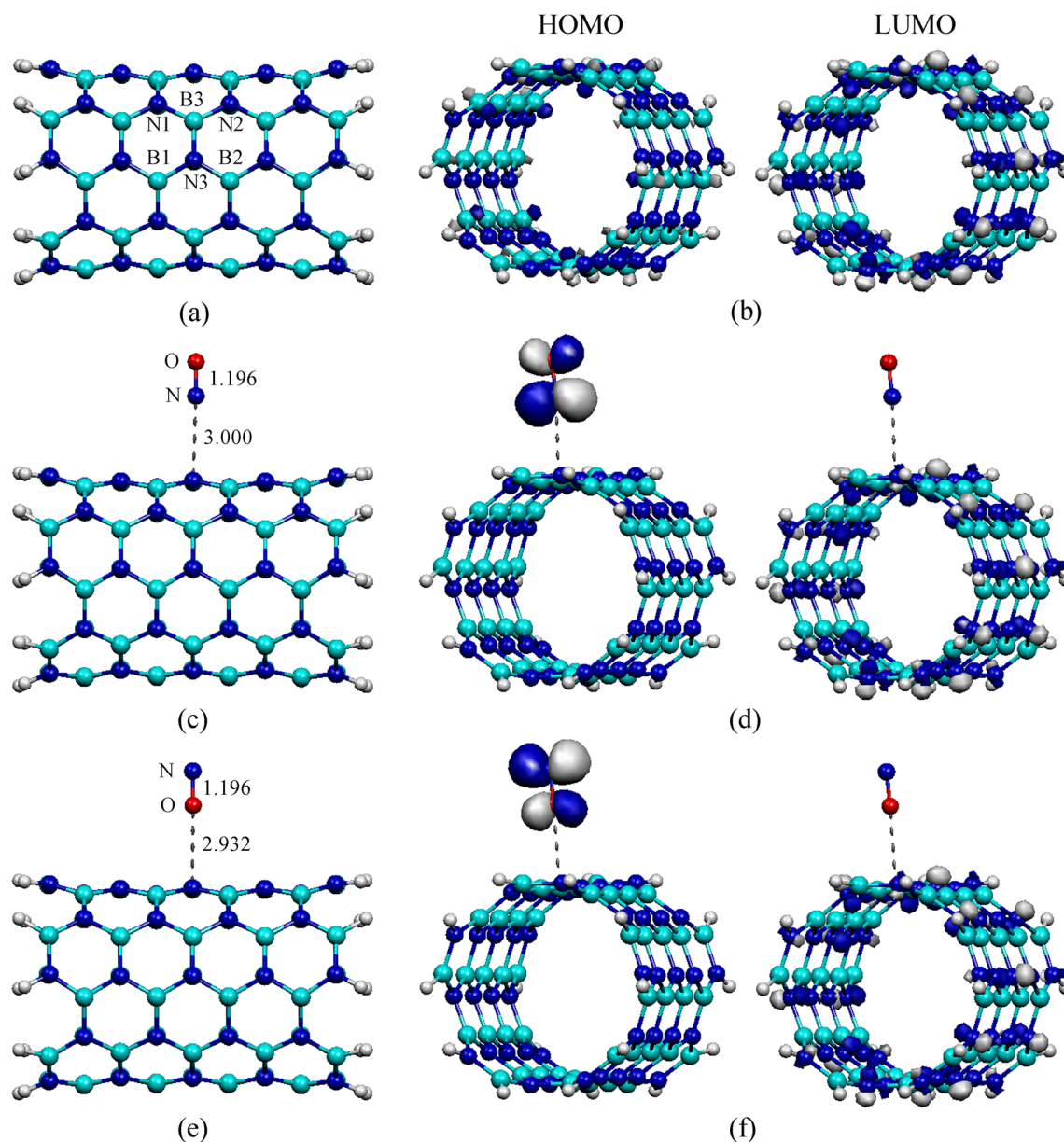
Fig. 1 The B3LYP/LanL2DZ optimized structures of **a** pristine BNNT, **c** NO, and **e** NO adsorbed on pristine BNNT and the plots of HOMO and LUMO density distributions of **b** pristine BNNT, **d** NO, and **f** NO adsorbed on pristine BNNT. Bond lengths and adsorption distances are in Å

respectively. The large ADs indicate that NO molecule can undergo weakly physical adsorption on the pristine BNNT via the van der Waals force. For the NO/TM_B-doped BNNTs, the ADs between the NO molecule and TM_B-doped BNNTs are in the range of 1.672–1.908 Å (NO adsorptions) and 1.754–1.961 Å (NO adsorptions), as shown in Figs. 4 and 5, respectively. For the NO/TM_N-doped BNNTs, the ADs between the NO molecule and TM_N-doped BNNTs are in the range of 1.688–1.901 Å (NO adsorptions) and 1.757–2.001 Å (NO adsorptions), as shown in Figs. 6 and 7, respectively. The short ADs of NO/TM-doped BNNTs demonstrate that the adsorption abilities of NO/TM–doped BNNTs could be stronger than that of the NO/BNNT. It is also clear that the NO molecule prefers to adsorb on TM-doped BNNT systems. Therefore, a TM atom doping on BNNT shows that the adsorption ability of NO molecule is significantly improved. In addition, the N–O bond lengths of NO/TM-doped BNNTs (1.219–1.384 Å) lead to elongation in comparison with an isolated NO molecule (1.199 Å), which are also consistent with the previous study of N–O bond length for NO adsorption on C- (1.230 Å) [54], Si- (1.210 Å) [55], and V-doped BNNTs (1.210 Å) [34]. These imply that the adsorption process displays weaken the N–O bond of NO molecule (Figs. 4, 5, 6 and 7).
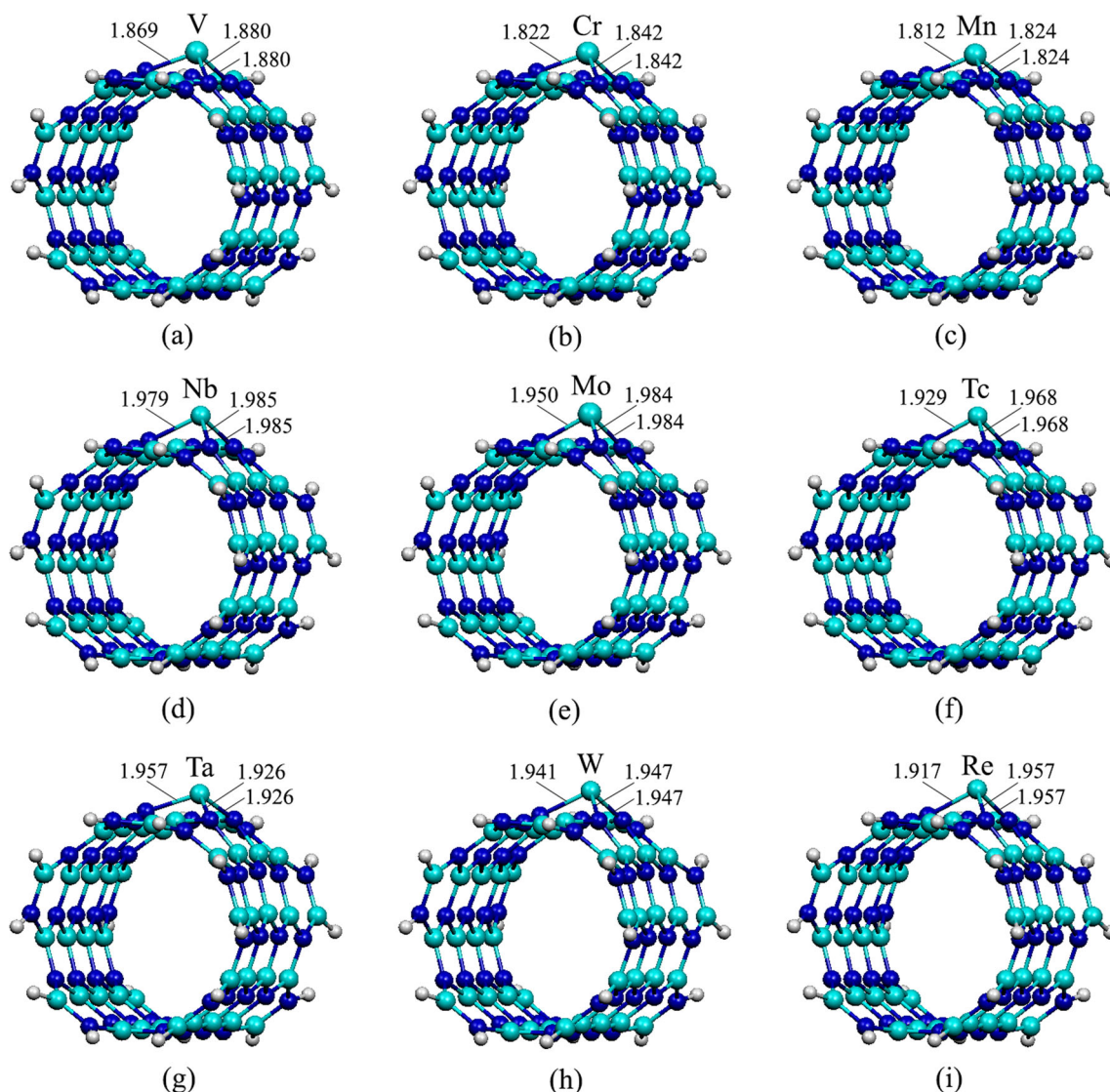
Fig. 2 The B3LYP/LanL2DZ optimized structures of **a** V_B-, **b** Cr_B-, **c** Mn_B-, **d** Nb_B-, **e** Mo_B-, **f** Tc_B-, **g** Ta_B-, **h** W_B-, and **i** Re_B-doped BNNTs

Binding energies of TM atom doping on BNNT and adsorption energies of NO molecule adsorbed on pristine and TM-doped BNNTs

The reactivities of TM atoms on the nanotube were considered from the calculated binding energies (E_b), which are summarized in Table 1. The negative values of E_b imply that the interaction for TM atoms with BNNT surface corresponds to the exothermic and thermodynamically favorable. Thus, the binding interactions between TM atoms and BNNT are energetically favorable. Besides, it is also shown that the E_b values of TM_B-doped BNNTs and TM_N-doped BNNTs are in the range of − 269.69 to − 222.35 kcal/mol and − 190.88 to − 96.01 kcal/mol, respectively. These values confirm that the E_b values for TM_B-doped BNNTs have larger than those of TM_N-doped BNNTs, indicating that the TM_B-doped BNNTs show strong interaction in comparison with the TM_N-doped

BNNTs. In which, the Mo interacting with BNNT is much larger than that the other TM atoms for both two doping sites. Therefore, the large binding energy shows a strong binding interaction to form a stable complex. These results are in good agreement with previous studies for TM atoms doping on carbon nanotube [43], silicon carbide nanotube [44], aluminum nitride nanotube, and other nanostructures [1, 3].

The adsorption energies (E_{ads}) of NO molecule adsorbed on the pristine and TM-doped BNNTs are listed in Tables 2 and 3. As can be seen, the E_{ads} values of NO molecule adsorbed via its N and O atoms toward the pristine BNNT are calculated to be − 4.01 and − 2.76 kcal/mol, respectively. The small E_{ads} value indicates that the pristine BNNT is slightly sensitive to the NO molecule that corresponds to the large AD and small PCT values. The E_{ads} values of NO/TM_B-doped BNNTs and NO/TM_N-doped BNNTs are in the range of − 105.66 to − 48.22 kcal/mol and − 97.24 to − 59.15 kcal/mol,
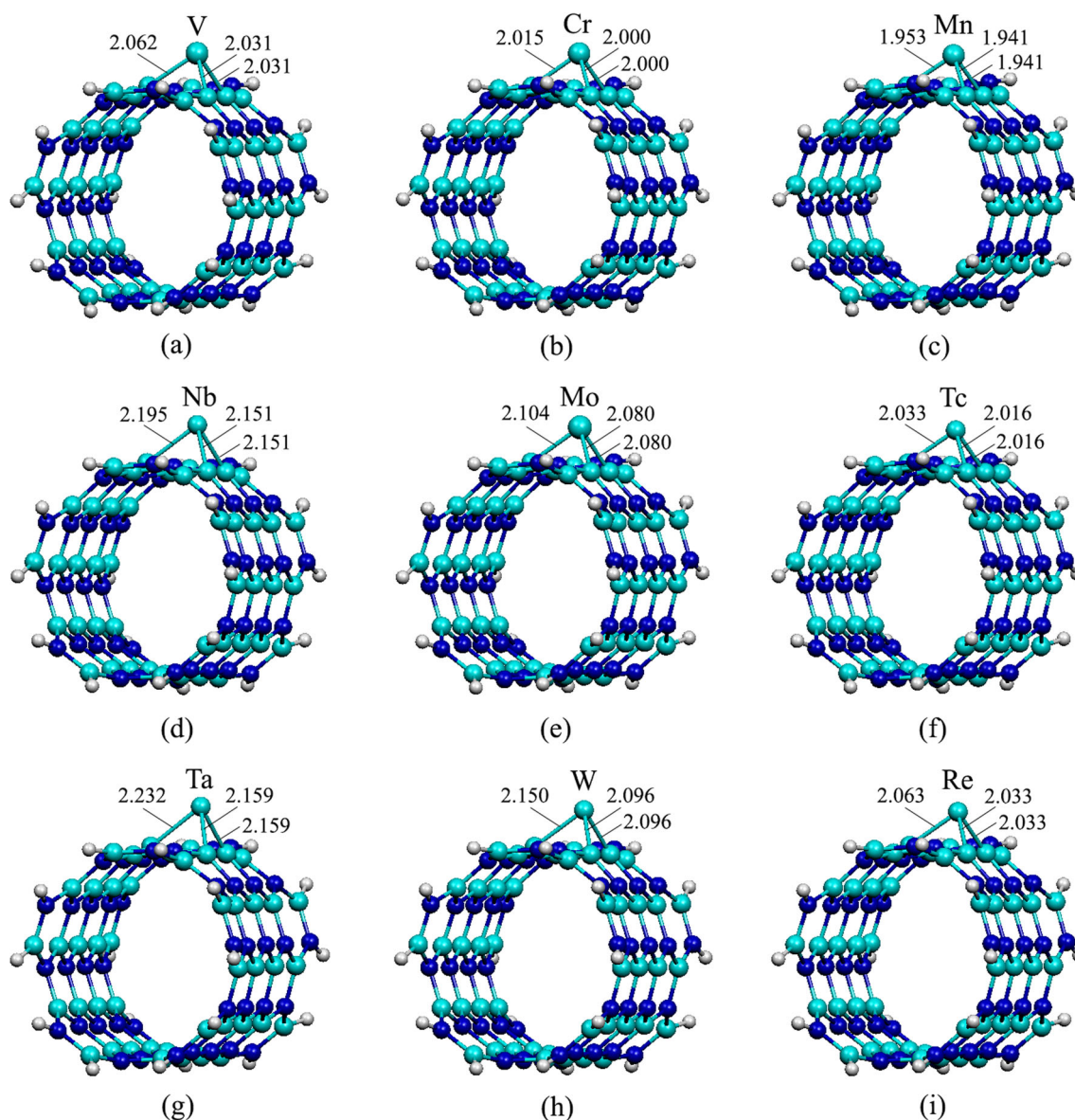
Fig. 3 The B3LYP/LanL2DZ optimized structures of **a** V_N-, **b** Cr_N-, **c** Mn_N-, **d** Nb_N-, **e** Mo_N-, **f** Tc_N-, **g** Ta_N-, **h** W_N-, and **i** Re_N-doped BNNTs

respectively. Whereas, the E_{ads} values of NO/TM_B-doped BNNTs and N$\underline{O}$/TM_N-doped BNNTs are found to be − 83.05 to − 11.50 kcal/mol and − 81.96 to − 17.45 kcal/mol, respectively. For the NO/TM_B-doped BNNTs, the Re_B- and Ta_B-doped BNNTs display stronger interaction with NO molecule than the other TM atoms when pointing its N and O atom toward the adsorption site, respectively. For the NO/TM_N-doped BNNTs, the Mn_N-doped BNNT displays much stronger interaction with NO molecule than other TM atoms for both its N and O atoms toward the adsorption site. Also, the adsorption ability of NO/TM_B-doped BNNT systems displays higher than those of the NO/TM_N-doped BNNT systems except for NO/Cr-doped BNNT and NO/Mn-doped BNNT. Thus, the adsorption abilities of NO molecule on the BNNT are outstandingly improved through doping with TM atoms,

which were previously investigated and confirmed by NO adsorption on V-, Cr-, Mn-, Fe-, Co-, and Ni-doped BNNTs [34]. Furthermore, all E_{ads} values of NO adsorption via N atom toward the TM-doped BNNTs ($\underline{N}$O/TM-doped BNNT) are higher than the NO adsorption via O atom toward the TM-doped BNNTs (N$\underline{O}$/TM-doped BNNT), indicating that the NO adsorption via N atom toward the TM-doped BNNTs is more stable than the adsorption via O atom toward the TM-doped BNNTs. The N atom of NO molecule toward the adsorption sites presents an energetically favorable adsorption configuration, which is in good accordance with previous research for NO adsorption on the Ge-doped BNNT [35]. Based on these calculated results, the BNNT becomes strong interaction toward the NO molecule after impurity doping, and TM atoms play a crucial role in capturing the NO molecule.
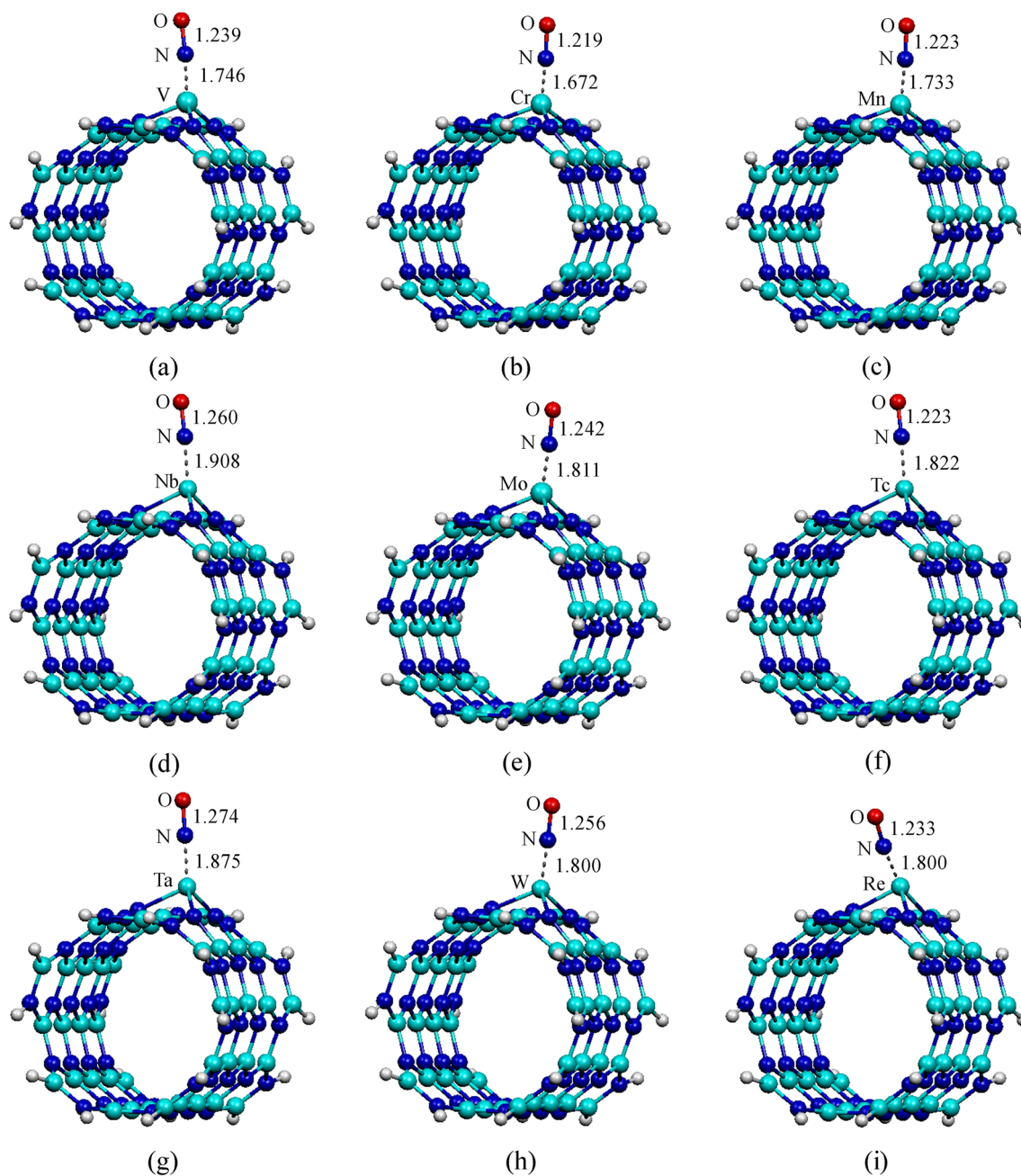
Fig. 4 The B3LYP/LanL2DZ optimized structures of **a** $\underline{N}O/V_B$-, **b** $\underline{N}O/Cr_B$-, **c** $\underline{N}O/Mn_B$-, **d** $\underline{N}O/Nb_B$-, **e** $\underline{N}O/Mo_B$-, **f** $\underline{N}O/Tc_B$-, **g** $\underline{N}O/Ta_B$-, **h** $\underline{N}O/W_B$-, and **i** $\underline{N}O/Re_B$-doped BNNTs

Electronic properties of pristine and TM-doped BNNTs and their NO adsorptions

The sensitivity of the V-, Cr-, Mn-, Nb-, Mo-, Tc-, Ta-, W-, and Re-doped BNNTs to the gas molecule could be related to the energy gaps, charge transfers, and total density of states (DOSs). Natural bond orbital (NBO) analysis was performed to evaluate electron transfer before and after NO adsorption. The partial charge transfers (PCTs) during the adsorption process of pristine or TM-doped BNNT with NO molecule were also calculated and presented in Tables 2 and 3. The PCTs are defined as $Q_{NO/BNNT} - Q_{NO}$ and $Q_{NO/TM\text{-}BNNT} - Q_{NO}$ where $Q_{NO/BNNT}$ and $Q_{NO/TM\text{-}BNNT}$ are the total charge of NO molecule adsorbed on the pristine and TM-doped BNNT, respectively, and Q_{NO} is the total charge of NO molecule in isolate system. According to the obtained PCT results, the PCTs between NO molecule and pristine BNNT are 0.023 and 0.019 e for $\underline{N}O/BNNT$ and $N\underline{O}/BNNT$, respectively; these indicate that partial charge is slightly transferred from nanotube to NO molecule. As NO interacts with TM-doped BNNTs, PCTs for these systems are mainly negative values (− 0.544 to −
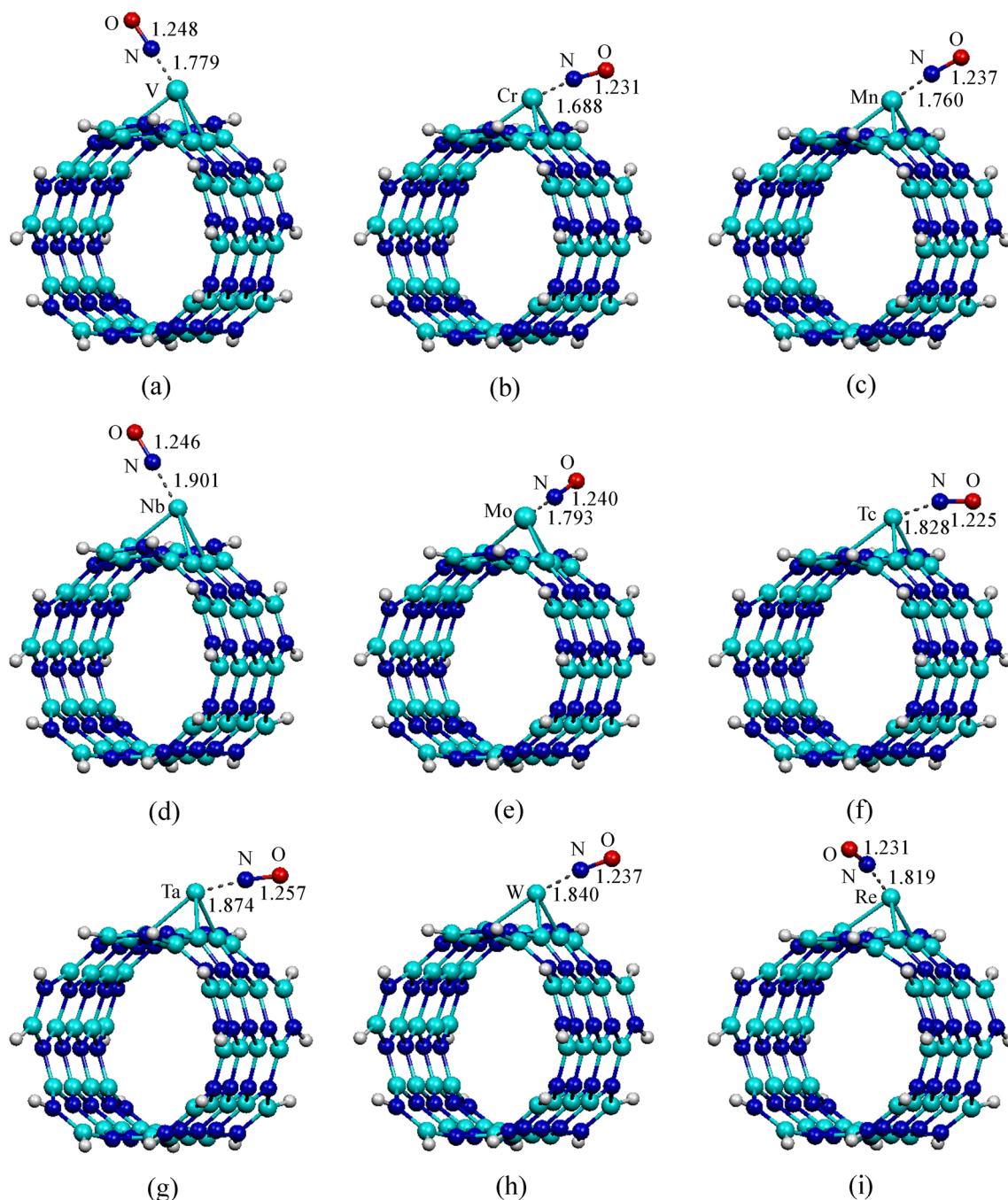
Fig. 5 The B3LYP/LanL2DZ optimized structures of **a** $\underline{N}O/V_{N}$-, **b** $\underline{N}O/Cr_{N}$-, **c** $\underline{N}O/Mn_{N}$-, **d** $\underline{N}O/Nb_{N}$-, **e** $\underline{N}O/Mo_{N}$-, **f** $\underline{N}O/Tc_{N}$-, **g** $\underline{N}O/Ta_{N}$-, **h** $\underline{N}O/W_{N}$-, and **i** $\underline{N}O/Re_{N}$-doped BNNTs

0.042 e), in which the charges are also transferred from the NO to the TM-doped BNNTs, except for NO adsorbed on Cr_B-doped BNNT, the PCT is a positive value (0.104 e). The large charge transfers can be explained that the electronegativities of N and O atoms of NO molecule are larger than that of TM atom on the nanotube, thus leading the former to attract TM atom. The interactions between NO molecule and TM-doped BNNTs prove the nature. The TM atoms could also be contributed the electron of the

dangling bond binding interaction with the NO molecule, thus charge transfers between TM-doped BNNT and NO molecule are determined. This supported the notion that the TM-doped BNNTs can be strongly sensitive to NO molecule than the pristine BNNT.

For the most stable configuration of pristine and TM-doped BNNTs and their NO adsorptions, we examined the highest occupied molecular orbital energies (E_{HOMO}), the lowest unoccupied molecular orbital energies (E_{LUMO}), and
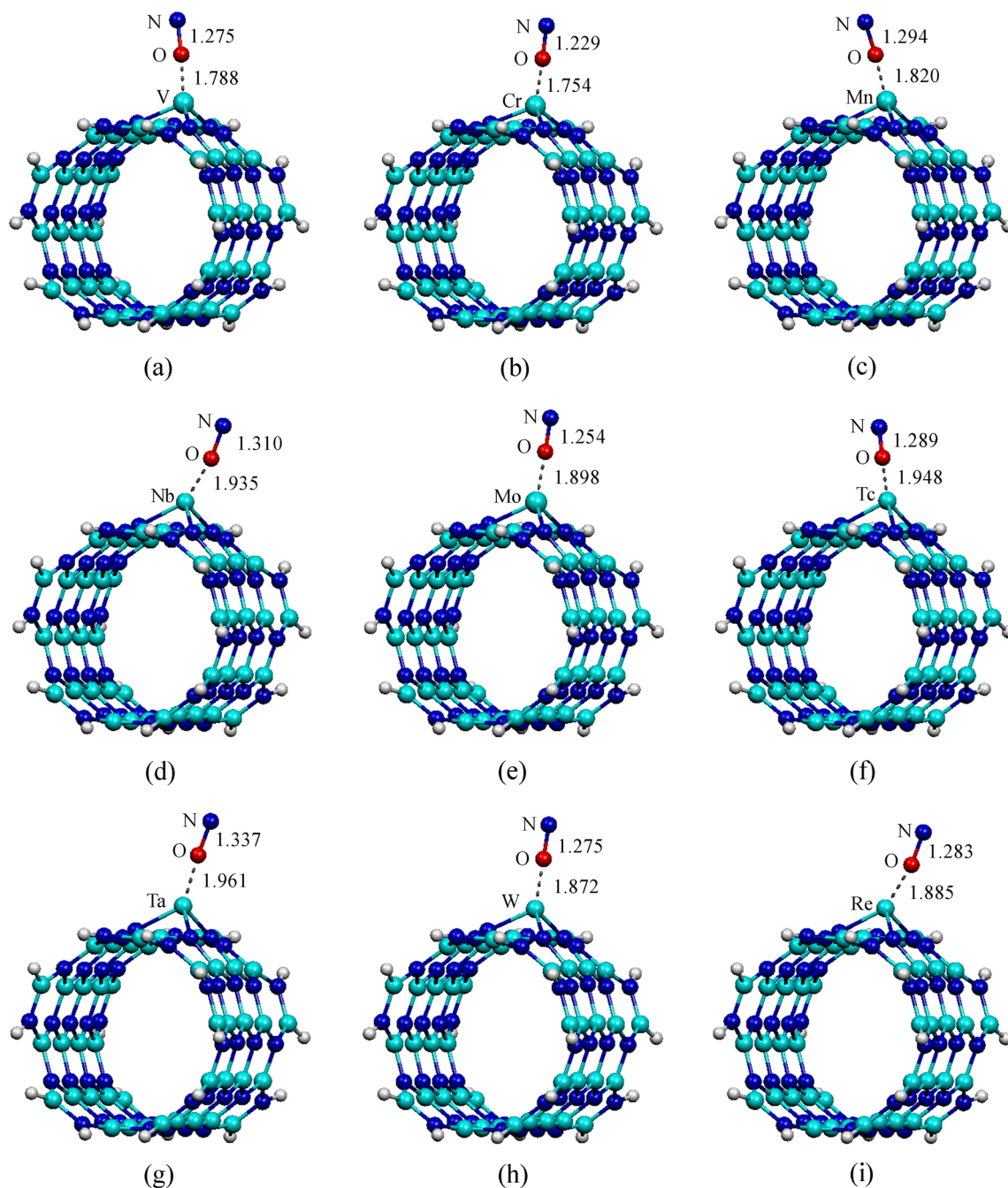
Fig. 6 The B3LYP/LanL2DZ optimized structures of **a** N<u>O</u>/V$_B$-, **b** N<u>O</u>/Cr$_B$-, **c** N<u>O</u>/Mn$_B$-, **d** N<u>O</u>/Nb$_B$-, **e** N<u>O</u>/Mo$_B$-, **f** N<u>O</u>/Tc$_B$-, **g** N<u>O</u>/Ta$_B$-, **h** N<u>O</u>/W$_B$-, and **i** N<u>O</u>/Re$_B$-doped BNNTs

the energy gaps (E_g). The results of which are listed in Tables 1, 2, and 3. It is found that the calculated E_g for TM$_B$-doped BNNTs and TM$_N$-doped BNNTs are in the range of 1.361–2.476 and 1.796–3.211 eV, respectively, which are significant smaller than the E_g of the pristine BNNT (6.013 eV). In which, the E_g of the pristine BNNT presents in good agreement with data obtained from the theoretical (6.10 eV) [56] and experimental studies (5.50 eV) [57]. Thus, the TM atoms doping can induce

dramatically decrease in the E_g of nanotube, in which the chemical reactivities of TM-doped BNNTs are also increased. These are in complete agreement with Pt atom doping on BNNT as reported by Dong *et al.* [58]. Upon exposure to the NO molecule, the E_g of the N<u>O</u>/BNNT and NO/BNNT are found to be 3.374 and 2.939 eV, respectively. For the NO/TM-doped BNNT systems, the significant changes in E_g of TM-doped BNNTs after NO adsorptions are found. Overall, we expected that the change in E_g
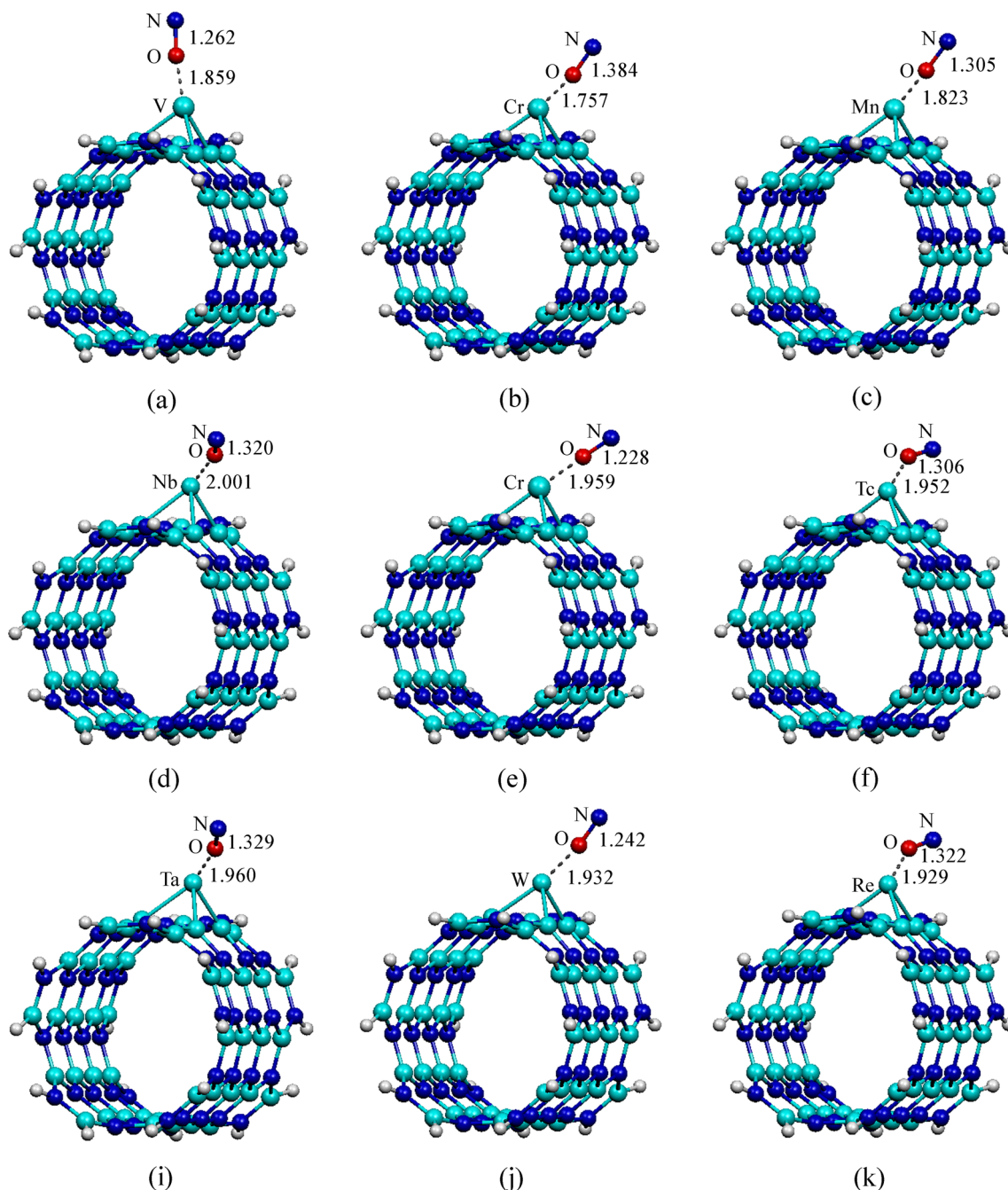
Fig. 7 The B3LYP/LanL2DZ optimized structures of **a** NO/V$_N$-, **b** NO/Cr$_N$-, **c** NO/Mn$_N$-, **d** NO/Nb$_N$-, **e** NO/Mo$_N$-, **f** NO/Tc$_N$-, **g** NO/Ta$_N$-, **h** NO/W$_N$-, and **i** NO/Re$_N$-doped BNNTs

would change the electrical conductivity of TM-doped BNNTs and NO/TM-doped BNNTs. Therefore, this relationship can be given by the following equation:

$$\sigma \propto \exp\left(\frac{-E_g}{2k_B T}\right) \quad (7)$$

where σ is the electric conductivity and k_B is the Boltzmann constant. According to the equation, the electrical

conductivity is exponentially related to E_g value. Therefore, a small decrease in E_g leads to higher electrical conductivity at a given temperature. As can be seen in the change of energy gaps (ΔE_g) in Table 1, it is shown that the TM$_B$-doped BNNTs display higher change of energy gaps (3.537–4.652 eV) than that of the TM$_N$-doped BNNTs (2.802–4.217 eV). This large reduction of E_g (or high ΔE_g) will exponentially raise the population of conductance electrons based on the Eq. 7. Whereas, the change of ΔE_g for NO/TM-doped BNNTs

Table 1 Binding energies (E_b), the highest occupied molecular orbitals (E_{HOMO}), the lowest unoccupied molecular orbitals (E_{LUMO}), energy gaps (E_g), changes of energy gaps (ΔE_g), and TM charges of pristine and TM-doped BNNTs

Species	E_b[a]	E_{HOMO}[b]	E_{LUMO}[b]	E_g[b]	ΔE_g[b, d]	TM charge[c]
BNNT	–	– 6.612	– 0.599	6.013	–	B = 1.224
						N = – 1.224
V_B–BNNT	– 246.94	– 4.517	– 2.694	1.823	4.190	1.129
Cr_B–BNNT	– 273.92	– 5.442	– 3.075	2.367	3.646	0.996
Mn_B–BNNT	– 222.35	– 5.959	– 3.483	2.476	3.537	0.994
Nb_B–BNNT	– 262.46	– 3.565	– 2.177	1.388	4.625	1.266
Mo_B–BNNT	– 296.69	– 4.272	– 2.912	1.361	4.652	1.101
Tc_B–BNNT	– 238.32	– 5.007	– 3.401	1.605	4.408	0.951
Ta_B–BNNT	– 285.33	– 3.293	– 1.742	1.551	4.462	1.317
W_B–BNNT	– 289.65	– 3.946	– 2.531	1.415	4.598	1.187
Re_B–BNNT	– 256.35	– 4.626	– 3.129	1.497	4.516	1.017
V_N–BNNT	– 96.01	– 4.680	– 2.340	2.340	3.673	0.211
Cr_N–BNNT	– 135.01	– 4.517	– 2.095	2.422	3.591	0.134
Mn_N–BNNT	– 97.66	– 5.279	– 2.068	3.211	2.802	– 0.019
Nb_N–BNNT	– 128.08	– 4.653	– 2.857	1.796	4.217	0.366
Mo_N–BNNT	– 190.88	– 4.816	– 2.585	2.231	3.782	0.077
Tc_N–BNNT	– 159.99	– 5.279	– 2.612	2.667	3.346	– 0.169
Ta_N–BNNT	– 140.16	– 4.953	– 2.884	2.068	3.945	0.491
W_N–BNNT	– 181.07	– 5.143	– 2.884	2.259	3.754	0.253
Re_N–BNNT	– 180.40	– 5.361	– 3.102	2.259	3.754	– 0.019

[a] In kilocalories/mol (kcal/mol)

[b] In electron volt (eV)

[c] In electron (e)

[d] ΔE_g defined as $E_{g(BNNT)} - E_{g(TM–BNNT)}$

induces the change in the electrical conductivity of the tube, as listed in Tables 2 and 3.

The other chemical reactivity indices, chemical hardness and electrophilicity, were also considered for our systems. The chemical hardness is the resistance of a chemical species to change in electronic configuration. It is implied that increasing in chemical hardness leads to an increase of stability and diminish of reactivity for the systems. The chemical indices for pristine and TM-doped BNNTs and their NO adsorptions are presented in Tables S3–S5. The results show that the chemical hardness for the pristine BNNT is calculated to be 3.01 eV, whereas TM_B-doped BNNTs and TM_N-doped BNNTs are in the range 0.69–1.24 and 0.90–1.61 eV, respectively. When NO approaches to the outer surface of the TM-doped BNNTs, it can be concluded that almost chemical hardness values are decreased and electrophilicity values are increased in comparison with NO adsorption on the pristine BNNT (Tables S4 and S5), leading to their reactivity of the systems increasing. Therefore, TM atoms can improve the molecular reactivity of NO adsorbed on the nanotube.

Furthermore, the HOMO and LUMO orbital distributions of pristine and TM-doped BNNTs and their NO adsorptions are also investigated. The plots of the HOMO and LUMO orbital distributions of pristine BNNT and

NO/BNNT are displayed in Fig. 1b, d, and f. As can be seen, the HOMO and LUMO orbitals of the pristine BNNT are delocalized around the tube. Whereas, the HOMO orbitals of the NO/BNNTs are delocalized on NO molecule and the LUMO orbitals are delocalized around the tube, suggesting that the LUMO is not contributed to the adsorption process. The HOMO and LUMO orbital distributions of TM-doped BNNTs are localized on TM doping sites (Figs. S1 and S2). While, the HOMO and LUMO orbital distributions for the NO/TM-doped BNNT systems are localized throughout the doping and adsorption sites, suggesting the electron conduction through these systems, as displayed in Figs. S3–S6.

To better understand the electronic properties of the systems, the total electronic density of states (DOSs) for the pristine and TM-doped BNNTs and their NO adsorptions were plotted and observed. The DOS plots before and after NO adsorption on pristine BNNT are displayed in Fig. 8a and d. As can be seen, the DOS analysis indicates that the pristine BNNT exhibits a symmetry distribution between spin up and spin down channels with a large band gap of 6.013 eV. After TM doping on the nanotube, the DOS plot of BNNT not only shifts to another energy region but also appear new impurity states in their band gap region, in which the DOSs of these

Table 2 Adsorption energies (E_{ads}), E_{HOMO}, E_{LUMO}, E_g, ΔE_g, and partial charge transfers (PCTs) of NO molecule adsorbed on pristine and TM-doped BNNTs

Species	E_{ads}[a]	E_{HOMO}[b]	E_{LUMO}[b]	E_g[b]	ΔE_g[b, d]	PCTs[c]
NO/BNNT	− 4.01	− 6.612	− 3.238	3.374	− 2.640	0.023
NO/V$_B$–BNNT	− 80.77	− 5.69	− 3.619	2.150	0.327	− 0.121
NO/Cr$_B$–BNNT	− 48.22	− 6.204	− 3.619	2.585	0.218	0.104
NO/Mn$_B$–BNNT	− 75.91	− 6.422	− 4.027	2.395	− 0.082	− 0.117
NO/Nb$_B$–BNNT	− 92.55	− 5.225	− 3.184	2.041	0.653	− 0.403
NO/Mo$_B$–BNNT	− 79.60	− 5.769	− 3.048	2.721	1.361	− 0.223
NO/Tc$_B$–BNNT	− 82.87	− 6.313	− 3.646	2.667	1.061	− 0.100
NO/Ta$_B$–BNNT	− 104.98	− 4.980	− 2.857	2.123	0.571	− 0.532
NO/W$_B$–BNNT	− 104.23	− 5.388	− 2.667	2.721	1.306	− 0.403
NO/Re$_B$–BNNT	− 105.66	− 6.068	− 3.401	2.667	1.170	− 0.218
NO/V$_N$–BNNT	− 80.50	− 5.197	− 2.531	2.667	0.327	− 0.303
NO/Cr$_N$–BNNT	− 64.95	− 5.823	− 2.558	3.265	0.844	− 0.129
NO/Mn$_N$–BNNT	− 97.24	− 5.987	− 2.476	3.510	0.299	− 0.113
NO/Nb$_N$–BNNT	− 59.15	− 4.653	− 2.531	2.123	0.327	− 0.361
NO/Mo$_N$–BNNT	− 72.43	− 5.633	− 2.367	3.265	1.034	− 0.188
NO/Tc$_N$–BNNT	− 70.10	− 6.095	− 2.884	3.211	0.544	− 0.138
NO/Ta$_N$–BNNT	− 67.60	− 5.306	− 3.238	2.068	0.000	− 0.437
NO/W$_N$–BNNT	− 74.25	− 5.878	− 3.265	2.612	0.354	− 0.309
NO/Re$_N$–BNNT	− 71.92	− 6.095	− 3.510	2.585	0.327	− 0.223

[a] In kcal/mol

[b] In eV

[c] In e

[d] ΔE_g defined as $E_{g(NO/BNNT)} - E_{g(BNNT)}$ or $E_{g(NO/TM–BNNT)} - E_{g(TM–BNNT)}$

systems are induced to reduce the band gap successively, as displayed in Figs. S7 and S8. This confirms that the DOS of pristine BNNT increased the conductivity owing to the presence of TM atoms. For the DOS of NO adsorption on BNNT, it is revealed that the DOS of NO/BNNT is slightly changed by NO adsorption, which indicates low sensible effect on the electronic properties of the tube. After NO adsorption on TM-doped BNNTs, the DOSs of TM-doped BNNTs are also significantly changed with unsymmetry distributions (Figs. S9–S12), except for NO/Cr-, NO/Mo-, and NO/W-doped BNNTs, in which the DOSs of NO/Mo-doped BNNTs are displayed in Fig. 8b, c, e, and f. As mentioned above, it can be concluded that these changes in the DOSs are beneficial for gas sensing application.

Table 3 Adsorption energies (E_{ads}), E_{HOMO}, E_{LUMO}, E_g, ΔE_g, and PCTs of NO molecule adsorbed on pristine and TM-doped BNNTs

Species	E_{ads}[a]	E_{HOMO}[b]	E_{LUMO}[b]	E_g[b]	ΔE_g[b, d]	PCTs[c]
NO/BNNT	− 2.76	− 6.612	− 3.674	2.939	− 3.075	0.019
NO/V$_B$–BNNT	− 54.84	− 5.089	− 3.102	1.986	− 0.354	− 0.258
NO/Cr$_B$–BNNT	− 11.50	− 5.796	− 3.810	1.986	− 0.435	− 0.042
NO/Mn$_B$–BNNT	− 62.74	− 6.177	− 3.864	2.313	− 0.898	− 0.426
NO/Nb$_B$–BNNT	− 61.74	− 5.089	− 3.048	2.041	0.245	− 0.495
NO/Mo$_B$–BNNT	− 34.20	− 5.197	− 3.238	1.959	− 0.272	− 0.304
NO/Tc$_B$–BNNT	− 54.58	− 6.041	− 3.456	2.585	− 0.082	− 0.250
NO/Ta$_B$–BNNT	− 83.05	− 4.381	− 2.449	1.932	− 0.136	− 0.544
NO/W$_B$–BNNT	− 49.06	− 4.735	− 2.748	1.986	− 0.272	− 0.464
NO/Re$_B$–BNNT	− 54.64	− 5.415	− 3.048	2.367	0.109	− 0.335
NO/V$_N$–BNNT	− 45.97	− 5.170	− 2.912	2.259	− 0.082	− 0.292
NO/Cr$_N$–BNNT	− 43.21	− 5.850	− 2.884	2.966	0.544	− 0.175
NO/Mn$_N$–BNNT	− 81.96	− 5.442	− 2.721	2.721	− 0.490	− 0.479
NO/Nb$_N$–BNNT	− 51.01	− 5.089	− 3.048	2.041	0.245	− 0.457
NO/Mo$_N$–BNNT	− 17.45	− 5.306	− 2.966	2.340	0.109	− 0.222
NO/Tc$_N$–BNNT	− 34.07	− 5.578	− 2.966	2.612	− 0.054	− 0.332
NO/Ta$_N$–BNNT	− 53.48	− 5.143	− 3.265	1.878	− 0.190	− 0.479
NO/W$_N$–BNNT	− 24.50	− 5.878	− 3.265	2.612	0.354	− 0.287
NO/Re$_N$–BNNT	− 42.15	− 5.714	− 3.102	2.612	0.354	− 0.350

[a] In kcal/mol

[b] In eV

[c] In e

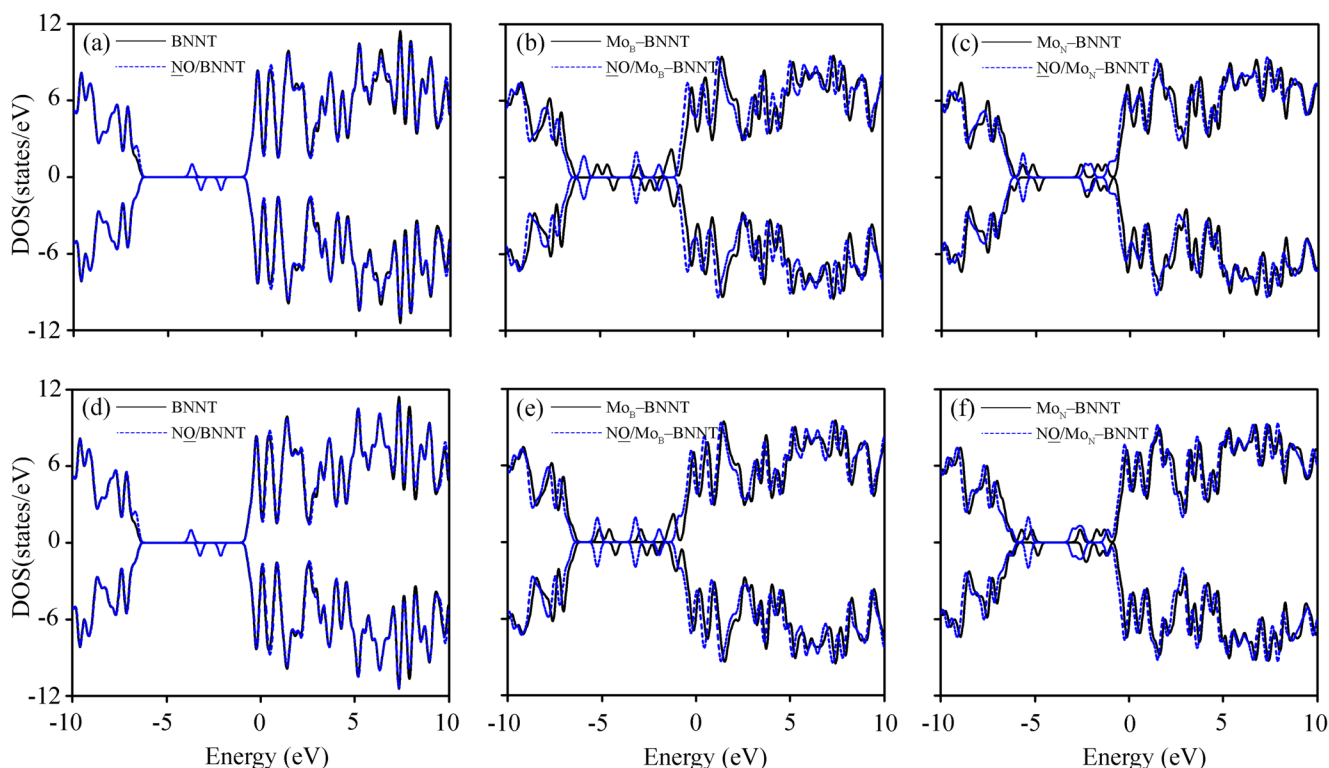[d] ΔE_g defined as $E_{g(NO/BNNT)} - E_{g(BNNT)}$ or $E_{g(NO/TM–BNNT)} - E_{g(TM–BNNT)}$

Fig. 8 DOSs of NO molecule adsorption on **a** pristine, **b** Mo$_B$-, and **c** Mo$_N$-doped BNNTs and DOSs of NO molecule adsorption on **d** pristine, **e** Mo$_B$-, and **f** Mo$_N$-doped BNNTs

Conclusions

The adsorptions of NO molecule onto the pristine and TM-doped BNNTs were investigated using the density functional theory method. The structural properties, electronic properties, and adsorption abilities for the most stable configuration of NO adsorptions on pristine and TM-doped BNNTs were calculated. The binding energies of TM-doped BNNTs reveal that the Mo atom doping exhibits the strongest binding ability with BNNT. In addition, the NO molecule weakly interacts with the pristine BNNT, whereas it has a strong adsorption ability on TM-doped BNNTs. The increase in the adsorption ability of NO molecule onto the TM-doped BNNTs is due to the geometrical deformation on TM doping site and the charge transfer between TM-doped BNNTs and NO. Moreover, a significant decrease in energy gap of the BNNT after TM doping is expected to be an available strategy for improving its electrical conductivity. These observations suggest that NO adsorption and sensing ability of BNNT could be drastically improved by introducing appropriate TM dopant. Therefore, TM-doped BNNTs can be used as advancing novel material for reliable and efficient NO storage and sensing.

References

1. Esrafili MD, Heydari S (2018) Carbon−doped boron−nitride fullerenes as efficient metal−free catalysts for oxidation of SO$_2$: a DFT study. Struct Chem 29:275

2. Muniyandi S, Sundaram R, Kar T (2018) Aluminum doping makes boron nitride nanotubes (BNNTs) an attractive adsorbent of hydrazine (N$_2$H$_4$). Struct Chem 29:375

3. Wanno B, Tabtimsa C (2014) A DFT investigation of CO adsorption on VIIIB transition metal–doped graphene sheets. Superlattice Microst 67:110

4. Roy S, Baiker A (2009) NO$_x$ storage–reduction catalysis : from mechanism and materials properties to storage–reduction performance. Chem Rev 109:4054

5. Aplincourt P, Bohr F, Ruiz–Lopez MF (1998) Density functional studies of compounds involved in atmospheric chemistry: nitrogen oxides. J Mol Struct 426:95

6. Yamini Y, Moradi M (2014) Influence of topological defects on the nitrogen monoxide-sensing characteristics of graphene–analogue BN. Sensors Actuators B Chem 197:274

7. Promthong N, Nunthaboot N, Wanno B (2015) A DFT study of CO and NO adsorptions on AlN–, AlP–, and ZnO–doped graphene nanosheets. Z Phys Chem 230:267

8. Chandiramouli R, Srivastava A, Nagarajan V (2015) NO adsorption studies on silicene nanosheet : DFT investigation. Appl Surf Sci 351:662

9. Deng ZY, Zhang JM, Xu KW (2016) Adsorption of SO₂ molecule on doped (8, 0) boron nitride nanotube: a first–principles study. Phys E 76:47

10. Esrafili MD, Saeidi N (2016) DFT calculations on the catalytic oxidation of CO over Si–doped (6,0) boron nitride nanotubes. Struct Chem 27:595

11. Singla P, Singhal S, Goel N (2013) Theoretical study on adsorption and dissociation of NO₂ molecules on BNNT surface. Appl Surf Sci 283:881

12. Esrafili MD, Saeidi N (2017) N₂O + SO₂ reaction over Si– and C–doped boron nitride nanotubes: a comparative DFT study. Appl Surf Sci 403:43

13. Rubio A, Corkill JL, Cohen ML (1994) Theory of graphitic boron nitride nanotubes. Phys Rev B 49:5081

14. Blase X, Rubio A, Louie SG, Cohen ML (1994) Stability and band gap constancy of boron nitride nanotubes. Europhys Lett 28:335

15. Chopra NG, Luyken RJ, Cherrey K, Crespi VH, Cohen ML, Louie SG, Zettl A (1995) Boron nitride nanotubes. Science 269:966

16. Zhi C, Bando Y, Tan C, Golberg D (2005) Effective precursor for high yield synthesis of pure BN nanotubes. Solid State Commun 135:67

17. Wang J, Kayastha VK, Yap YK, Fan Z, Lu JG, Pan Z, Ivanov IN, Puretzky AA, Geohegan DB (2005) Low temperature growth of boron nitride nanotubes on substrates. Nano Lett 5:1

18. Juárez AR, Anota EC, Cocoletzi HH, Ramírez JFS, Castro M (2017) Stability and electronic properties of armchair boron nitride/carbon nanotubes. Fuller Nanotub Car N 12:716

19. Chopra NG, Zettl A (1998) Measurement of the elastic modulus of a multi−wall boron nitride nanotube. Solid State Commun 105:297

20. Lan H, Ye L, Zhang S, Peng L (2009) Transverse dielectric properties of boron nitride nanotubes by ab initio electric field calculations. Appl Phys Lett 94:183110

21. Chang CW, Fennimore AM, Afanasiev A, Okawa D, Ikuno T, Garcia H, Li D, Majumdar A, Zettl A (2006) Isotope effect on the thermal conductivity of boron nitride nanotubes. Phys Rev Lett 97:85901

22. Chen Y, Zou J, Campbell SJ, Caer GL (2004) Boron nitride nanotubes : pronounced resistance to oxidation. Appl Phys Lett 84:2430

23. Zhi C, Bando Y, Tang C, Xie R, Sekiguchi T, Golberg D (2005) Perfectly dissolved boron nitride nanotubes due to polymer wrapping. J Am Chem Soc 127:15996

24. Zhi C, Bando Y, Tang C, Golberg D (2006) Engineering of electronic structure of boron–nitride nanotubes by covalent functionalization. Phys Rev B 74:153413

25. Chen X, Wu P, Rousseas M, Okawa D, Gartner Z, Zettl A, Bertozzi CR (2009) Boron nitride nanotubes are noncytotoxic and can be functionalized for interaction with proteins and cells. J Am Chem Soc 131:890

26. Ahmadi A, Beheshtian J, Hadipour N (2011) Chemisorption of NH₃ at the open ends of boron nitride nanotubes: a DFT study. Struct Chem 22:183

27. Lauret JS, Arenal R, Ducastelle F, Loiseau A, Cau M, Attal–Tretout B, Rosencher E, Goux–Capes L (2005) Optical transitions in single–wall boron nitride nanotubes. Phys Rev Lett 94:37405

28. Soltani A, Raz SG, Rezaei VJ, Dehno Khalaji A, Savar M (2012) Ab initio investigation of Al– and Ga–doped single–walled boron nitride nanotubes as ammonia sensor. Appl Surf Sci 263:619

29. Movlarooy T, Fadradi MA (2018) Adsorption of cyanogen chloride on the surface of boron nitride nanotubes for CNCl sensing. Chem Phys Lett 700:7

30. Beheshtian J, Ahmadi A, Bagheri Z (2012) Detection of phosgene by Sc–doped BN nanotubes : a DFT study. Sensors Actuators B Chem 171–172:846

31. Deng Z, Zhang J, Xu K (2015) First–principles study of SO₂ molecule adsorption on the pristine and Mn–doped boron nitride nanotubes. Appl Surf Sci 347:485

32. Tang C, Bando Y, Ding X, Qi S, Golberg D (2002) Catalyzed collapse and enhanced hydrogen storage of BN nanotubes. J Am Chem Soc 124:14550

33. Xie Y, Zhang JM (2011) First–principles study on substituted doping of BN nanotubes by transition metals V, Cr, and Mn. Comput Theor Chem 976:215

34. Xie Y, Huo YP, Zhang JM (2012) First–principles study of CO and NO adsorption on transition metals doped (8,0) boron nitride nanotube. Appl Surf Sci 258:6391

35. Wang R, Zhang D, Liu C (2014) The germanium–doped boron nitride nanotube serving as a potential resource for the detection of carbon monoxide and nitric oxide. Comput Mater Sci 82:361

36. Mananghaya M, Yu D, Santos GN (2016) Hydrogen adsorption on boron nitride nanotubes functionalized with transition metals. Int J Hydrog Energy 41:13531

37. Azizi K, Salabat K, Seif A (2014) Methane storage on aluminum–doped single wall BNNTs. Appl Surf Sci 309:54

38. Becke AD (2014) A new mixing of Hartree–Fock and local density–functional theories. J Chem Phys 98:1372

39. Becke AD (1988) Density–functional exchange−energy approximation with correct asymptotic behavior. Phys Rev A 38:3098

40. Becke AD (1993) Density–functional thermochemistry. III. The role of exact exchange. J Chem Phys 98:5648

41. Hay PJ, Wadt WR (1985) Ab initio effective core potentials for molecular calculations. Potentials for the transition metal atoms Sc to Hg. J Chem Phys 82:270

42. Wadt WR, Hay PJ (1985) Ab initio effective core potentials for molecular calculations. Potentials for main group elements Na to Bi. J Chem Phys 82:284

43. Buasaeng P, Rakrai W, Wanno B, Tabtimsai C (2017) DFT investigation of NH₃, PH₃, and AsH₃ adsorptions on Sc–, Ti–, V–, and Cr–doped single–walled carbon nanotubes. Appl Surf Sci 400:506

44. Baei MT, Bagheri Z, Peyghan AA (2013) Transition metal atom adsorptions on a boron nitride nanocage. Struct Chem 24:1039

45. Kaewruksa B, Ruangpornvisuti V (2011) Theoretical study on the adsorption behaviors of H₂O and NH₃ on hydrogen–terminated ZnO nanoclusters and ZnO graphene–like nanosheets. J Mol Struct 994:276

46. Vessally E, Dehbandi B, Edjlali L (2016) DFT study on the structural and electronic properties of Pt–doped boron nitride nanotubes. Russ J Phys Chem A 90:1217

47. Foster JP, Weinhold F (1980) Natural hybrid orbitals natural hybrid orbitals. J Am Chem Soc 102:7211

48. Frisch MJ, Trucks GW, Schlegel HB, Scuseria GE, Robb MA, Cheeseman JR, Montgomery Jr JA, Vreven T, Kudin KN, Burant JC, Millam JM, Iyengar SS, Tomasi J, Barone V, Mennucci B, Cossi M, Scalmani G, Rega N, Petersson GA, Nakatsuji H, Hada M, Ehara M, Toyota K, Fukuda R, Hasegawa J, Ishida M, Nakajima T, Honda Y, Kitao O, Nakai H, Klene M, Li X, Knox JE, Hratchian HP, Cross JB, Bakken V, Adamo C, Jaramillo J, Gomperts R, Stratmann RE, Yazyev O, Austin AJ, Cammi R, Pomelli C, Ochterski JW, Ayala PY, Morokuma K, Voth GA, Salvador P, Dannenberg JJ, Zakrzewski VG, Dapprich S, Daniels AD, Strain MC, Farkas O, Malick DK, Rabuck AD, Raghavachari K, Foresman JB, Ortiz JV, Cui Q, Baboul AG, Clifford S, Cioslowski J, Stefanov BB, Liu G, Liashenko A, Piskorz P, Komaromi I, Martin RL, Fox DJ, Keith T, AleLaham MA, Peng

CY, Nanayakkara A, Challacombe M, Gill PMW, Johnson B, Chen W, Wong MW, Gonzalez C, Pople JA (2009) GAUSSIAN 09, Revision A.02. Gaussian Inc, Wallingford CT

49. Flükiger P, Lüthi HP, Portmann S (2000) MOLEKEL 4.3. Swiss Center for Scientific Computing, Manno, Switzerland

50. O'Boyle NM, Tenderholt AL, Langner KM (2008) Software news and updates cclib : a library for package–independent computational chemistry algorithms. J Comput Chem 29:839

51. Parr RG, Donnelly RA, Levy M, Palke WE (1978) Electronegativity: the density functional viewpoint. J Chem Phys 68:3801

52. Koopmans T (1934) Über die zuordnung von wellenfunktionen und eigenwerten zu den einzelnen elektronen eines atoms. Physica 1: 104

53. Parr RG, Szentpaly LV, Liu S (1999) Electrophilicity index. J Am Chem Soc 121:1922

54. Baierle RJ, Schmidt TM, Fazzio A (2007) Adsorption of CO and NO molecules on carbon doped boron nitride nanotubes. Solid State Commun 142:49

55. Esrafili MD, Saeidi N (2015) Si–embedded boron-nitride nanotubes as an efficient and metal-free catalyst for NO oxidation. Superlattice Microst 81:7

56. Tontapha S, Ruangpornvisuti V, Wanno B (2013) Density functional investigation of CO adsorption on Ni-doped single-walled armchair (5,5) boron nitride nanotubes. J Mol Model 19:239

57. Arenal R, Ferrari AC, Reich S, Wirtz L, Mevellec JY, Lefrant S, Rubio A, Loiseau A (2006) Raman spectroscopy of single–wall boron nitride nanotubes. Nano Lett 6:1812

58. Dong Q, Li XM, Tian WQ, Huang XR, Sun CC (2010) Theoretical studies on the adsorption of small molecules on Pt-doped BN nanotubes. J Mol Struct 948:83